Collision Induced Unfolding Reveals Disease-Associated Stability Shifts in Mitochondrial tRNAs

Anna G. Anders[1], Elizabeth D. Tidwell[2], Varun V. Gadkari[3], Markos Koutmos[1,2], and Brandon T. Ruotolo[1]

1 Department of Chemistry, University of Michigan, Ann Arbor, Michigan 48109, United States

2 Department of Biophysics, University of Michigan, Ann Arbor, Michigan 48109, United States

3 Department of Chemistry, University of Minnesota, Minneapolis, Minnesota 55455, United States

KEYWORDS: Ion mobility-mass spectrometry, Native Mass Spectrometry, Structural Biology, Mitochondria, MELAS, tRNA

––ABSTRACT: Ribonucleic acids (RNAs) remain challenging targets for structural biology, creating barriers to understanding their vast functions in cellular biology and fully realizing their applications in biotechnology. The inherent dynamism of RNAs creates numerous obstacles in capturing their biologically relevant higher-order structures (HOSs), and as a result, many RNA functions remain unknown. In this report, we describe the development of native ion mobility-mass spectrometry (IM-MS) and collision induced unfolding (CIU) for the structural characterization of a variety of RNAs. We evaluate the ability of these techniques to preserve native structural features into the gas-phase across a wide range of functional RNAs. Finally, we apply these tools to study the elusive mitochondrial encephalopathy, lactic acidosis, and stroke-like episodes (MELAS)-associated A3243G mutation. Our data demonstrate that our experimentally determined conditions preserve some solution-state memory of RNA via the increasing complexity of CIU fingerprints by RNA HOS and the retention of predicted magnesium binding events. Relating to the role of MELAS-inducing mutations in mitochondrial transfer RNA (mt-tRNAs), significant differences in collision cross-section (CCS) and stability are observed as a function of the A3243G mutation across a subset of the mitochondrial transfer RNA (tRNA) maturation pathway. We conclude by discussing the potential application of CIU for the development of RNA-based biotherapeutics and, more broadly, transcriptomic characterization.

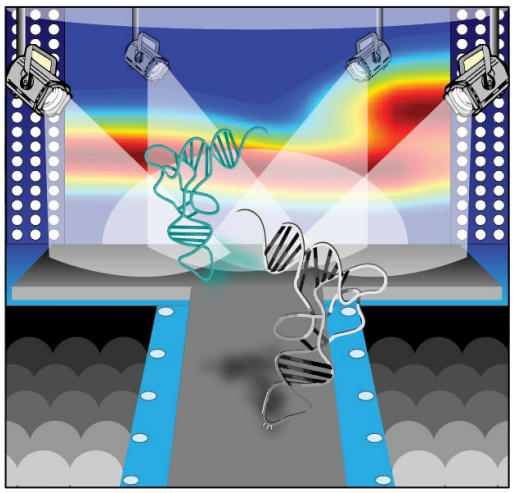

INTRODUCTION

It was not until the completion of the Human Genome Project (HGP) that the breadth of RNA species and their respective functions began to be realized.[1-3] To the surprise of many, most of the human genome did not encode for proteins but rather for RNAs that carry out key biological functions or possess unknown roles in cellular biochemistry.[1] Since this discovery, a surge in RNA structural biology has followed, and the utility this molecular class possesses in biotherapeutic development continues to expand.[4,5] These studies have brought to light the wide range of RNA sequence lengths and types, the extensive post-transcriptional modifications (PTMs) required for their native functions, the structural dynamism inherent to these biomolecules, and the manner in which both their structures and their functions depend upon solution conditions.[6-9] However, many of the biophysical techniques utilized for these aforementioned studies require copious amounts of sample, extensive preparation, long analysis times, and often sacrifice the native dynamism of the RNA species probed.

These challenges demand the development of new technologies capable of studying the higher-order structures (HOSs) of these non-coding RNAs (ncRNAs) both at biologically-relevant concentrations and under biologically-relevant conditions. Recently, ion mobility-mass spectrometry (IM-MS) has emerged as a useful structural biology tool, and its application to nucleic acids continues to show great promise.[1,10-13] In short, IM works by separating gas-phase ions by charge and rotationally averaged collision cross-sections (CCSs) within miliseconds.[14] In conjunction with MS, ions of the same mass-to-charge (m/z) ratio and different CCSs can be readily distinguished. Importantly for RNA, extensive structural dynamics do not restrict IM-MS measurements, enabling the inherent dynamism of these biomolecules to be probed directly.

Collision induced unfolding (CIU) has further enabled IM-MS to synchronously monitor analyte structures and stabilities[15] while providing domain-level structural insight.[16,17] Specifically, CIU experiments work by collisionally activating ions of interest to induce structural unfolding prior to IM separation. For proteinaceous characterization, CIU has proven powerful

in discriminating differences in disulfide-bond patterns of monoclonal antibodies, classifying kinase inhibitors, and capturing RNA binding protein (RNP) substrate dependencies.[18-20] However, the utility of CIU in probing nucleic acid structures remains unexplored.

In this report, we have improved the capability of IM-MS and CIU to capture native-like gas-phase nucleic acid ions across a wide range of structured ncRNAs. Specifically, we experimentally determined conditions to mitigate their gas-phase collapse and better preserve solution-state cationic bound states into the gas-phase. These conditions were applied to a mitochondrial transfer RNA (mt-tRNA) to robustly characterize its HOS through CCS and stability measurements recorded across mt-tRNA maturation and mutation states using CIU, for the first time. Our results both confirm prior measurements obtained from previous reports and add key measurements pertaining to as yet un-probed maturation states of the MELAS mt-tRNA leucine (Leu, UUR). Specifically, we observe that A3243G MELAS mutation confers a significant increase in CCS in immature pre-tRNAs containing the 5' leader sequence while producing more compact configurations across other tRNA states studied, suggesting a uniquely aberrant tertiary structure is adopted for A3243G sequences prior to RNaseP processing. Furthermore, we observe the greatest degree of destabilization conferred by A3243G mutation is associated with intermediately-processed tRNAs states, suggesting an uneven risk of MELAS tRNAs adopting non-native folds throughout post-transcriptional processing. We conclude our report by discussing the implications of both CIU technologies for the study of RNA structure and function, as well as the potential importance of our MELAS mt-tRNA$^{Leu(UUR)}$ findings.

EXPERIMENTAL

Sample Preparation. Solid phase synthesized wild type (WT) and A3243G mutant mitochondrial transfer RNA (mt-RNA) were purchased from Integrated DNA Technologies (IDT) and supplied as lyophilized powder. All purchased RNAs were reconstituted using Milli-Q water (Millipore), aliquoted at 30uL 18uM stocks, and stored at -80C. The flavin mononucleotide riboswitch aptamer (FMNRS) was *in vitro* transcribed (IVT) using recombinant T7 RNA polymerase and a DNA oligonucleotide template ordered from IDT (Table S3).[21] RNA was transcribed from single stranded antisense DNA templates containing two 5' O-methyl modifications annealed to a short complementary T7 promoter oligo.[22] Transcriptions were carried out at 37C with orbital shaking at 300 rpms in 40 mM Tris base pH 7.9, 2 mM spermidine, 0.01% Triton-X 100, 30 mM $MgCl_2$, 10 mM DTT, 7.11 mM ATP, 7.70mM CTP, 10.07 mM GTP, 7.11 mM UTP, 3% DMSO, 0.7uM T7 RNA polymerase, 0.5 U/mL inorganic pyrophosphatase (Thermo Fisher Scientific), and 0.1uM DNA template containing the T7 promoter sequence. After 3.75-4 hours reactions were quenched with EDTA and brought to pH at a final concentration of 60 mM. The resulting RNA was analyzed for quality and homogeneity using 12% polyacrylamide gel electrophoresis followed by either UV back shadowing[23] or staining using methylene blue.[24] The transcription reactions, if sufficiently homogenous, were further purified by size exclusion chromatography (SEC) to remove free nucleotides, short transcription termination products, and T7 RNA polymerase. Transcription mix was buffer exchanged into denaturing SEC buffer (0.1 M Tris pH 7, 0.1 M Boric Acid, 0.2 mM EDTA, 5 M Urea) using Amicon spin column (30 kDa MWCO). Concentrated RNA was injected onto an equilibrated Superdex S200 15/300 column (GE Healthcare, now Cytiva) and eluted at a flow rate of 0.35 mL per minute. Using the ultraviolet (UV) chromatogram and polyacrylamide gel electrophoresis (PAGE) analysis, the most homogenous fractions were pooled, and buffer exchanged using a fresh Amicon spin column (30 kDa MWCO) into a storage buffer, either TBE or 50 mM Tris, 50 mM borate, 150 mM KCl, and aliquoted to 30-60 uL and flash frozen in liquid nitrogen before storage at -80C.

For MS analysis, all RNAs were diluted to a working concentration of 2 uM at 60 uL. RNAs were thawed on ice before refolding via thermal denaturation at 90C for 3 minutes followed by incubation at 37C in the presence of 0.5 mM $Mg(OAc)_2$ for 15 minutes, then cooled at room temperature for 10 minutes before transferring to ice. For Mg^{2+}-dependent folding experiments, concentrations of 0.0 mM to 15 mM $Mg(OAc)_2$ were used in place of 0.5 mM. To remove non-specifically bound Mg^{2+} ions, the folded RNAs were buffer exchanged into pH~7 100 mM AmOAc with Micro Biospin P-6 Micro columns (Bio-Rad, Hercules, CA). The modified single stranded short interfering RNA (siRNA) and siRNA Duplex (each 60 uL at 2 uM) were provided by Amgen (sequences are proprietary to Amgen) and did not undergo any refolding as described above.

High Resolution Mass Spectrometry. A ThermoFisher Q-Exactive Ultra high mass resolution (QE-UHMR) Hybrid Quadrupole-Orbitrap Mass Spectrometer was used for identifying Mg-bound populations of the mt-tRNA$^{Leu(UUR)}$ identified under a negative ionization polarity. Samples were buffer exchanged into 100 mM ammonium acetate (AmOAc) using Micro Bio-Spin P-6 gel columns (Bio-Rad, Hercules, CA) and directly infused via nanoelectrospray ionization (nESI).[25] nESI was performed using borosilicate needles pulled and coated in-house with a Sutter p-97 Needle Puller and a Quorum SCX7620 mini sputter coater, respectively. QE-UHMR acquisition settings can be found in Supplementary Table 1. The acquired native mass spectra were deconvoluted using UniDec in negative polarity.[26]

IM-MS and CIU. An Agilent 6560C (Agilent Technologies, Santa Clara, CA) was utilized for all IM-MS and CIU experiments where the instrument configuration has been previously described.[27,28] RNA samples were nanoelectrosprayed (capillary voltages of 1.2 kV – 1.5 kV) with in-house pulled borosilicate capillary needles. For higher in-source activation (>390 V), sulfur hexafluoride (SF_6) was used as a drying gas between the fragmentor (F) and capillary exit (CE) lenses to act an electron scavenger and prevent arcing. Additionally, SF_6(g) has a larger mass than the typical N_2 gas used in this region of the instrument and results in higher laboratory-frame energy collisions with the analyte ions. Throughout the rest of the instrument, high-purity nitrogen ($N_{2(g)}$) was used. Additional 6560C settings can be found in the supporting information (Table S2).

Multifield CCS measurements were conducted across 1450—1700 V (by 50 V increments) at the drift tube entrance voltage and collected in 0.5 min intervals. CIU experiments were conducted by increasing the CE lens (up to +490 V) relative to the F lens (400 V). Specifically, 10 V steps at 0.2 mins were acquired from 10 V CE to 480 V CE. The time segment feature was used in the Agilent Mass Hunter 10 Acquisition software to collect all activation steps in a single file. The MIDAC Agilent data extractor (packaged with CIUSuite2) was used to extract the arrival time distributions (ATDs) for the ions of interest from each time segment. The ATDs were plotted against the applied ΔV, referred to as collision voltage (CV), using CIUSuite2.3. Importantly, this version of CIUSuite2[29] is crucial for accurate fitting of the compaction transition observed in nucleic acid CIU.

CIU Data Processing. Beta-version CIUSuite2.3 was used for CIU analysis of all nucleic acids (Figure S1). Specifically, raw instrument files were loaded via CIU batch extraction to generate .raw files. Within the batch extraction template, upper and lower m/z values were specified by charge state, and t0(t-fix) and β (beta) values were provided. t0 and β were acquired by spraying Agilent tunemix in a negative ionization polarity. The resulting mass spectra were subsequently analyzed in IM-MS Browser 10, and the single-field CCS calculator was used to extract the drift times of each tunemix ion to obtain t0 (t-fix) and β (beta) values for CIU-CCS calibration. Additionally, high energy and non-time segmented (a value of "0") was specified for the extraction.

Resulting text _raw.csv files were then used as input for CIUSuite2 data processing, using a smoothing window size of 5 and 1 iteration (2D Savitzky-Golay). The data were interpolated by a factor of 2 and cropped in both axes to better visualize the resulting fingerprint. Data were plotted and underwent standard feature detection with "exclude feature" set to false for all CIU50 analyses reported here.

RESULTS AND DISCUSSION

Ribonucleic Acids Structurally Compact Prior to CIU

Prior reports have detailed the potential of CIU assays to probe the structures and stabilities of a variety of proteins and protein complexes.[15-20] Typical CIU experiments produce increased drift times or CCSs in a manner correlated with increases in collision voltage (CV), with some cavity-containing protein complexes observed to undergo compaction upon collisional activation.[30] In contrast, RNA ions routinely undergo an initial compaction step upon collisional activation prior to more-standard CIU, the extent of which can vary. However, when evaluated across ionization polarities, charge states, ion species, and levels of pre-CIU HOS, this compaction remains the most prominent aspect of RNA CIU datasets (Figure S2). MS evaluation across respective CIU features reveals there to be no change in RNA mass during compaction, thus suggesting that an alteration in RNA HOS is the most likely origin of the observed shift in RNA CCS values (Figure S3). Identifying the significance this structural compaction plays in RNA HOS remains an active area of research, but integrating our results with data from prior reports indicates that counterion condensation of nucleic acids to be a likely mechanism to describe RNA ion compaction during CIU.[31,32]

To identify solution conditions that could be applied to a variety of RNA species for IM-MS analyses, we evaluated a number of RNA species prepared across many AmOAc concentrations and ionization polarities (Figure S4). Previous work has revealed an ionic strength dependency to produce specific nucleic acid charge states and CCSs,[33] and these trends were reproduced in our RNA IM-MS screen. Taken together, these conditions were applied for CIU analyses with the goal of capturing native-like RNA HOSs (Figure 1). From a short-interfering RNA (siRNA) sequence to a tRNA exhibiting a complex tertiary structure, we observe an increase in the number of CIU features with the number of HOS elements (*e.g.,* stem-loops, hairpin turns), suggesting a correlation between the two. To begin to characterize and correlate CIU features to potential HOS-element level unfolding events, we undertook an in-depth analysis of structured RNAs via IM-MS, CIU, and native MS.

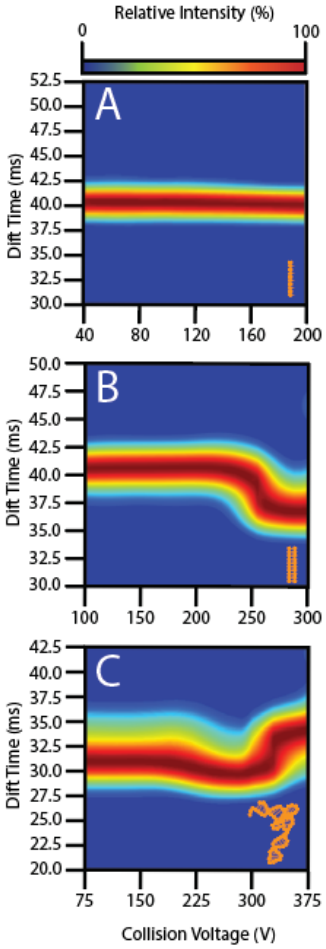

Figure 1. CIU detects HOSs in RNA species. Top to bottom (A-C), RNA species increase in their higher order structural complexity. (A) A single stranded short interfering RNA (siRNA) of primary structure. (B) An RNA duplex of secondary structure. (C) A mt-tRNA of tertiary structure. CIU analyses support the expected increase in HOS through the observed increasing number of features observed (n ≥3, RMSDs ≤ 2.00 for all).

IM-MS Preserves Native Mg^{2+}-Populations into the Gas Phase

Previous native MS work on nucleic acids has revealed that such ion species to undergo significant gas-phase collapse.[34,35] While these findings could suggest a loss of native-like structure upon desolvation, it has also been observed that nucleic acids can retain their specific cofactor interactions from the solution during MS analyses (Figure S5).[36-38] Prior gas-phase reports in this area have focused primarily on rigid nucleic acid structures. As such, the overall level of native higher order structural information preserved in the gas-phase for less rigid nucleic acid structures remains largely unknown.

We began recreating these previous experiments, and we further explored other reported solution conditions to discover which would adequately stabilize native-like RNA structures for IM-MS characterization. Ultimately, we found that solutions containing 100 mM AmOAc when ionized in a negative polarity mode were optimal for the IM-MS analyses of flexible RNAs. The ionic strength identified in our survey is lower than the optimal value reported previously for rigid nucleic acid species,[13] yet it was chosen for its ability to promote more native-like CCSs values in the RNA species studied here while preserving a native charge state envelope. The negative ionization polarity was selected for its ability to confer improved signal intensities for RNA species due to their greater anionic ionization efficiencies (Figure S4. A) and for the preservation of a native-net overall charge for RNA species, which can be a concern for the evaluation of biomolecular HOS, when compared to equivalent positive polarity datasets.

In addition to the considerations detailed above, various magnesium (Mg^{2+}) concentrations were explored in our evaluation of solution conditions designed to preserve native-like RNA HOS for IM-MS investigations. Mg^{2+} is a particularly important cofactor required for RNA structure, function, catalysis, and RNA binding proteins (RBPs).[39-41] In the context of RNA folding, Mg^{2+} concentrations vary extensively in solution-based folding protocols and commonly use magnesium chloride ($MgCl_2$).[42] Because free chloride (Cl^-) ions can lead to ion suppression in electrospray ionization, a $Mg(OAc)_2$ salt was chosen as a source of Mg^{2+} ions and for its MS-compatible counterion (acetate, OAc^-). Preliminary data collection was aimed at identifying if the solution structural Mg^{2+}-effects were retained in the gas-phase using a highly-structured flavin mononucleotide riboswitch (FMNRS) aptamer (Figure S6).[43] Upon the addition of micromolar amounts of $Mg(OAc)_2$ to RNA samples in solution, significant changes in both RNA CCS and stability were observed in our IM-MS data. Mg^{2+}-induced stabilization in RNA structures has been well reported in prior studies[44-47] and is reflected in CIU50 values that increase in a manner correlated with increasing $Mg(OAc)_2$ concentrations. However, given the non-linear nature of the correlation observed, we focused our efforts on determining the optimal amount of $Mg(OAc)_2$ for IM-MS and CIU characterization of structured and flexible RNA targets.

To identify optimal Mg^{2+} concentrations for native IM-MS studies of less rigid nucleic acid structures, a mt-tRNA (specifically, mt-$tRAN^{Leu(UUR)}$) was used as a model system. tRNAs as a whole often serve as model RNA systems due to their well-characterized solution-states, canonical secondary and tertiary structures (Figures 2A and S7),[48-50] and discrete structural-dependence on Mg^{2+} binding.[50] mt-tRNAs serve as unique tRNA species due to their hypothesized increase in dynamism when compared to cytosolic tRNAs.[51,52] Despite this increased dynamism, current literature identifies the presence of eight specifically bound Mg^{2+} ions for natively-structured tRNA,[51] and we have utilized native MS to determine if this stoichiometry is preserved for tRNA ions in the gas-phase.

Specifically, the canonical elbow-shaped, mature 3'CCA-containg wildtype synthesized mitochondrial (mt)-tRNA Leucine (LEU, UUR) was folded in concentrations of $Mg(OAc)_2$ ranging from 0.05 mM-10 mM in 100 mM AmOAc. As observed in our FMNRS data, we detect a stabilization and change in CCS upon the addition of $Mg(OAc)_2$ to mt-$tRNA^{Leu(UUR)}$ samples (Figure 2B). Our native MS data identify a plethora of Mg^{2+}:tRNA stoichiometries under the above-noted solution conditions, and as expected, with increasing Mg^{2+} concentrations in solution, we detect an increase in Mg^{2+}-binding/adduction to the RNA ions observed in our experiments. Despite this, we note that the weighted average of all Mg-bound RNA ion populations observed across all concentrations greater than ~25 μM produced values of 8 ± 1 Mg^{2+} ions bound (Figure 2C), with higher Mg-binding stoichiometries observed with insufficient intensity to significantly shift this average at higher Mg^{2+} concentrations. While the predicted stoichiometry was observed, it is important to note that there are two types of Mg^{2+}-RNA interaction – that of site-specific, tight binding for RNA folding and structure, and those that are non-specific in a secondary solvation shell serving as counter ions. Thus, while these mass spectrometry conditions may have captured the highly-specific and conserved Mg^{2+}-bound populations, the secondary Mg^{2+} ions have largely been lost. Aside from Mg^{2+}, it is further important to note that this ion is not the only cation involved in RNA structure. Cations such as sodium (Na^+) and potassium (K^+) are abundant within living cells, and these ions have been shown to be involved in several nucleic acid structures. Specifically, tRNAs have been identified to utilize Na^+ in addition to Mg^{2+}, and future work aims to address the concentrations of such ions needed for the improved analysis of native-like tRNAs in the absence of bulk solvent.

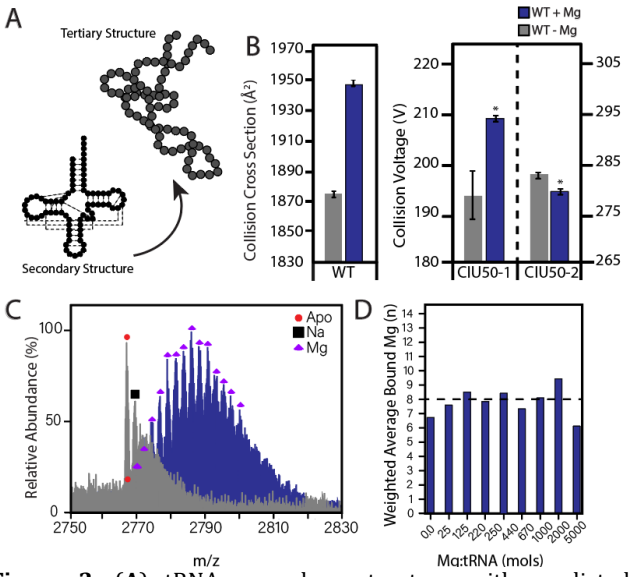

Figure 2. (**A**) tRNA secondary structure with predicted contacts to adopt the final tertiary structure. (**B**) CCS and CIU50 Mg^{2+}-dependences of the WT mt-$tRNA^{Leu(UUR)}$ species ($n \geq 3$, $p \leq 0.01$). (**C**) Native mass spectra of the Mg^{2+}-free 3'CCA species (grey) and a common Mg^{2+} folding concentration (blue). Adduct-free tRNAs are denoted by red cirlces, sodium adducts by black squares, and Mg^{2+} adducts by purple triangles. (**D**) Weighted averages of Mg^{2+}:tRNA as a function of $Mg(OAc)_2$ concentration ($n \geq 3$).

Shifts in MELAS-associated tRNA Structure and Stability

Human mitochondria are unique in that they contain their own genome and encode for a complete set of tRNAs separate from cytosolic tRNAs.[52] Importantly, these mt-tRNAs incur significant rates of mutation due to the highly oxidative environment native to the mitochondria, and these mutations result in several mitochondrial disorders that remain difficult to capture and characterize.[53-55]

Mitochondrial encephalopathy, lactic acidosis, and stroke-like episodes (MELAS) remain one of the most common, and often fatal, mitochondrial disorders beginning in early childhood, affecting both the nervous and muscular systems.[56] In approximately 80% of cases, an A3243G transition mutation occurring in the mt-$tRNA^{LEU(UUR)}$ is observed and correlated to the onset of the disorder.[57] While the current consensus is that this mutation negatively affects mitochondrial translation, the biophysical consequences of this mutation remain poorly understood.

Like cytosolic tRNAs, mt-tRNAs undergo 5' and 3' end processing, but these processing points differ in that mt-tRNAs are cleaved via the tRNA punctuation model unlike their cytosolic counterparts (Figure S8).[58] Currently, most prior work focusing on the A3243G MELAS RNA mutation has surrounded its ability to be processed by mitochondrial ribonuclease P (mt-RNAse P) at the 5'leader sequence,[41,59] but the effects the mutation induces across mt-tRNA maturation states have remained unexplored until now. Specifically, we leveraged the optimal solution and instrument conditions identified in the data described above for native-like gas-phase RNA analyses in

order to probe the biophysical consequences this mutation induces onto the mt-tRNAs across a subset of the RNA maturation pathway (Figure 3A).

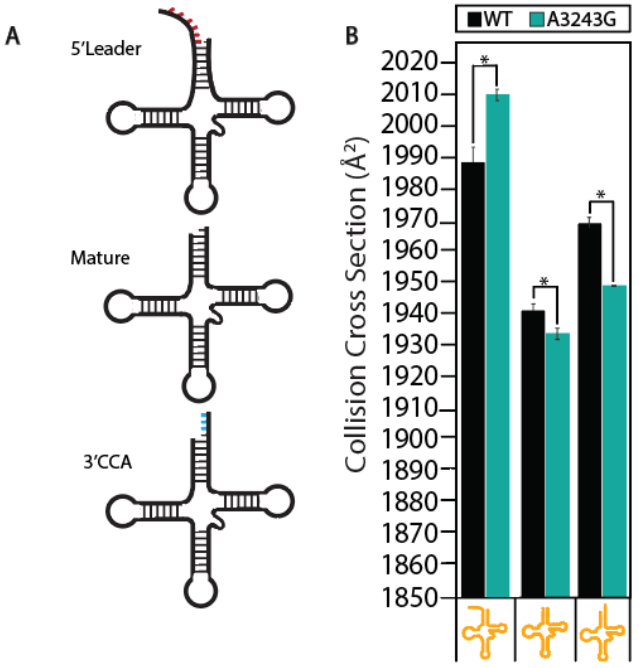

Figure 3. (**A**) Simplified mt-tRNA structure. Specifically, a 5'leader containing species (red), mature mt-tRNA, and a 3'CCA species (blue) were characterized in this work. It is important to note that following 3'CCA addition, these species are post-transcriptionally modified for mature functioning. (**B**) CCSs of the WT (black) and A3243G (turquoise) mt-tRNA$^{Leu(UUR)}$ across the maturation pathway (n=5, p≤0.005). Significant differences in CCS are observed across the mutation and the respective maturation species.

In agreement with previous A3243G-mutant results, an increase in RNA dimerization is observed for the 3'CCA containing species (Figure S9 A),[60] and for the first time, our data show an increase in dimerization for the 5'leader containing species (Figure S9 B). CCS data reveal significant differences across each point of maturation and mutation, but the overall effects these structural changes induce in the specific RNA species studied are difficult to interpret through CCS information alone (Figure 4A). Interestingly, it is important to note that while these changes in mt-tRNA CCS were not observed in the absence of Mg^{2+}, small differences in CIU were still able to be captured between RNA variants (Figure S10). In conjunction with CIU, we observe that the A3243G mutation destabilizes each mt-tRNA maturation state to a significant degree (Figure 4B). Likely, this destabilization stems from a hypothesized disruption of a conserved D-T loop interaction, an essential interaction for the adoption of proper tertiary structure (Figure 2A and S7). Taken together, the CCS data indicate a topological disruption in the mt-tRNA HOS while the CIU data confirms that A3243G mutation acts to destabilize the nucleic acid structure overall.

Interestingly, when our WT mt-tRNA IM-MS data is examined closely, unique trends are observed across the mt-tRNA maturation pathway. While the CCSs appear to be related to the overall mt-tRNA sequence length (where an increase in length likely relates to an increase in size), the trends in stability are more difficult to rationalize. The final addition of the 3'CCA confers greater stability than the longer 5'leader sequence while the species lacking both a 5'leader and 3'CCS is the most unstable. It is likely that specific nucleotides are contributing to the observed trends in RNA stability observed (e.g., canonical base pairing between the 6th nucleotide of the 5'leader with the 75th base of the 5'leader containing species), and future work investigating single-nucleotide truncations is needed to identify how these nucleotides affect the structure of each species. Finally, mt-tRNAs are highly dependent upon post-transcriptional modifications (PTMs) for proper structure and function (Figure S9).[61,62] The species in this work are solid-phase synthesized; thus, additional work exploring the post-transcriptionally modified maturation structures and the A3243G mutation are needed.

CONCLUSIONS

In this report, we have extensively characterized the utility of IM-MS and CIU to probe the HOS of large, dynamic nucleic acids. For the first time, CIU was utilized to probe RNA HOS, and our results indicate an overall increase in CIU fingerprint complexity as the number of discrete HOS elements are added to the structure. Additionally, CIU50 analyses recapitulate RNA stabilization and structural dependence on Mg^{2+}. Across each set of conditions tested, our results further demonstrate a unique and well-conserved structural compaction prior to unfolding in RNAs. While the overall level of compaction was found to be dependent upon HOS, charge-state, ion polarity, and solution conditions, it persists and is potentially a unique feature of gas-phase RNA CIU data.

In a more general sense, a set of conditions for the native IM-MS analysis of non-rigid RNAs were identified where these conditions proved to preserve Mg^{2+} specificity and ligand binding (i.e. FMN to the FMNRS) while mitigating gas-phase collapse. Gas-phase collapse was mitigated through a systemic identification of optimal solution conditions in terms of ionic strength and counter-ion concentrations. In agreement with previous work, an increase in CCS is observed with decreasing ionic strength in solution, and 100 mM AmOAc was ultimately chosen as it produced the most native-like CCS values without altering the native charge envelope of the RNA ions produced. These conditions were applied to a well-studied tRNA, and

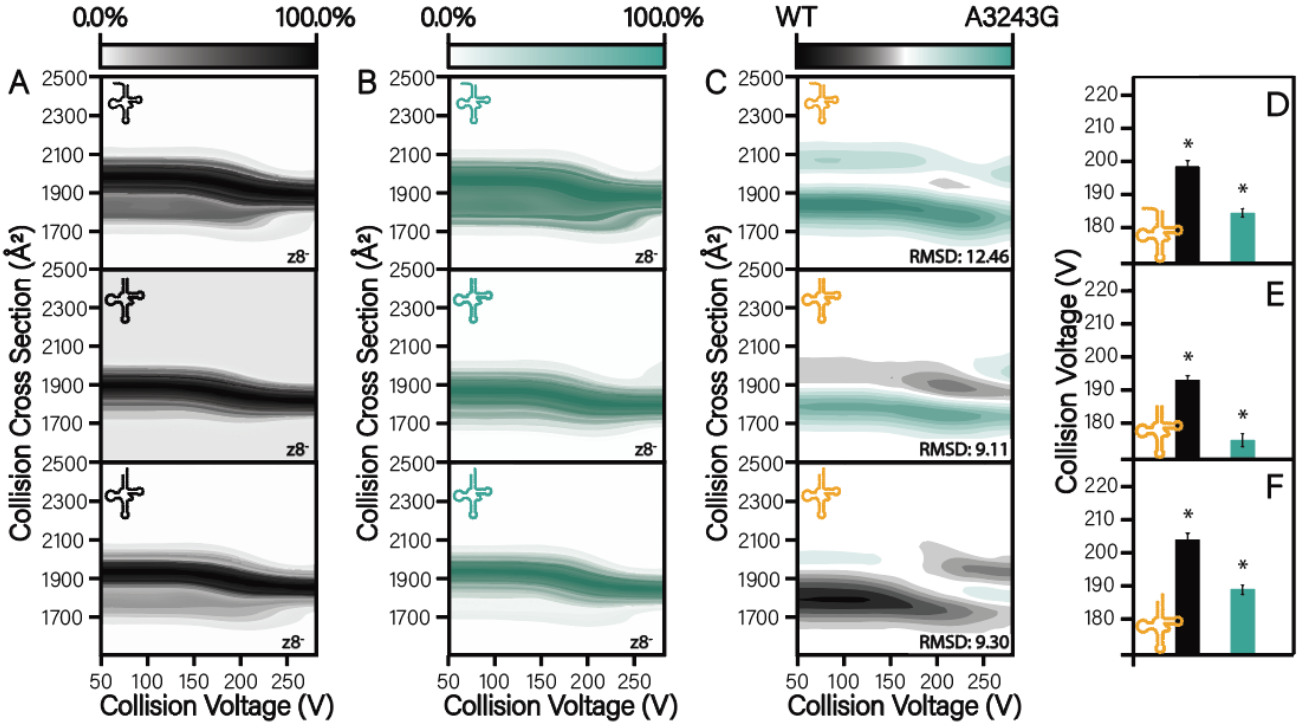

Figure 4. (**A**) Average CIU fingerprints of the WT (black) of the mt-tRNA$^{Leu(UUR)}$ in order of maturation (top to bottom). **(B)** Average CIU fingerprints of the A3243G mutant (teal) in order of maturation (top to bottom). **(C)** Average CIU fingerprints comparisons between the WT and A3243G species. **(D-F)** Compaction (CIU50-1) of the WT and A3243G mutant across maturation (top to bottom) (n ≥ 5 for all, replicate RMSDs ≤ 2.00, p ≤ 0.01).

ultimately observed to preserve specific bound states of the Mg^{2+} cofactor for the mt-tRNA$^{Leu(UUR)}$ species. Taken together, these conditions permitted the confident evaluation of the A3243G mutation, allowing us to quantify significant topological and stability differences across the mt-tRNA maturation pathway for this disease-associated nucleic acid.

Finally, these results indicate that some native-like properties of RNA HOSs are preserved in the gas-phase. Future research will be focused on the deployment of CIU to probe specific RNA secondary structures (e.g., hairpins, internal loops, pseudoknots, etc.) which could provide an informative roadmap for CIU fingerprint-interpretation. Furthermore, future work involving the characterization of the observed CIU50-1 compaction through a combination of solution, MS, and computational studies may provide new information surrounding RNA structure and poly-anionic gas phase species, in general.

AUTHOR INFORMATION

Corresponding Author

Brandon T. Ruotolo *– Department of Chemistry, University of Michigan, Ann Arbor, Michigan 48109, United States; orcid.org/0000-0002-6084-2328; Phone: 1-734- 615-0198; Email: bruotolo@umich.edu; Fax: 1-734-615- 3718*

Authors

Anna G. Anders *- Department of Chemistry, University of Michigan, Ann Arbor, Michigan 48109, United States. Orcid.org/0000-0002-4097-9650; Email: annaa@umich.edu*

Elizabeth Tidwell *– Department of Biophysics, University of Michigan, Ann Arbor, Michigan 48109, United States*

Varun V. Gadkari *– Department of Chemistry, University of Minnesota, Minneapolis, Minnesota 55455, United States*

Markos Koutmos *– Department of Biophysics, University of Michigan, Ann Arbor, Michigan 48109, United States*

Author Contributions

E.T and M.K. produced the FMNRS aptamer and provided guidance and background on native RNA structural studies. V.V.G. performed the initial FMNRS native MS/CIU experiments and advised further project direction/experimental design. M.K. further provided guidance surrounding mt-tRNAs and the A3243G mutation. A.G.A. collected all Agilent 6560C and QE-UHMR data and drafted the manuscript. B.T.R. and A.G.A. analyzed all data.

Notes

The authors declare no competing financial interest.

ACKNOWLEDGMENT

This work is supported by the Chemical Biology Training Program (CBTP; 5T32GM008353-30 to A.A), Agilent Technologies, the UM Biosciences Initiative, the National Institutes of Health (GM117141), and the National Science Foundation (1808541 and 2304961) Chemical Measurement and Imag-

ing Program with partial co-funding from the Division of Molecular and Cellular Biosciences. tRNA^{Ser}s were provided by Dr. Joshua Jones and Prof. Kristin Koutmou in the Department of Chemistry at the University of Michigan. The authors would like to thank Jennifer L. Lippens and Zhuoer Xie of Amgen Inc. for helpful discussions, and for providing siRNA samples.

ABBREVIATIONS

IM-MS, ion mobility-mass spectrometry; CIU, collision induced unfolding; mt-tRNA, mitochondrial transfer ribonucleic acid; FMNRS, flavin mononucleotide riboswitch; siRNA, short-interfering ribonucleic acid; MS, mass spectrometry; MELAS, mitochondrial encephalopathy, lactic acidosis, and stroke-like episodes; HOS, higher order structure; SEC, size exclusion chromatography; PAGE, polyacrylamide gel electrophoresis.

REFERENCES

(1) Valérie Gabelica. *Nucleic Acids in the Gas Phase*; Springer, 2014.
(2) Xu, B.; Zhu, Y.; Cao, C.; Chen, H.; Jin, Q.; Li, G.; Ma, J.; Yang, S. L.; Zhao, J.; Zhu, J.; Ding, Y.; Fang, X.; Jin, Y.; Kwok, C. K.; Ren, A.; Wan, Y.; Wang, Z.; Xue, Y.; Zhang, H.; Zhang, Q. C. Recent Advances in RNA Structurome. *Science China Life Sciences* **2022**, *65* (7), 1285–1324. https://doi.org/10.1007/s11427-021-2116-2.
(3) Xu, B.; Zhu, Y.; Cao, C.; Chen, H.; Jin, Q.; Li, G.; Ma, J.; Yang, S. L.; Zhao, J.; Zhu, J.; Ding, Y.; Fang, X.; Jin, Y.; Kwok, C. K.; Ren, A.; Wan, Y.; Wang, Z.; Xue, Y.; Zhang, H.; Zhang, Q. C. Recent Advances in RNA Structurome. *Science China Life Sciences* **2022**, *65* (7), 1285–1324. https://doi.org/10.1007/s11427-021-2116-2.
(4) Zhu, Y.; Zhu, L.; Wang, X.; Jin, H. RNA-Based Therapeutics: An Overview and Prospectus. *Cell Death & Disease* **2022**, *13* (7), 1–15. https://doi.org/10.1038/s41419-022-05075-2.
(5) Spitale, R. C.; Incarnato, D. Probing the Dynamic RNA Structurome and Its Functions. *Nature Reviews Genetics* **2022**, *24* (3), 178–196. https://doi.org/10.1038/s41576-022-00546-w.
(6) Ontiveros, R. J.; Stoute, J.; Liu, K. F. The Chemical Diversity of RNA Modifications. *Biochemical Journal* **2019**, *476* (8), 1227–1245. https://doi.org/10.1042/bcj20180445.
(7) Ganser, L. R.; Kelly, M. L.; Herschlag, D.; Al-Hashimi, H. M. The Roles of Structural Dynamics in the Cellular Functions of RNAs. *Nature Reviews Molecular Cell Biology* **2019**, *20* (8), 474–489. https://doi.org/10.1038/s41580-019-0136-0.
(8) Dai, X.; Zhang, S.; Zaleta-Rivera, K. RNA: Interactions Drive Functionalities. *Molecular Biology Reports* **2019**, *47* (2), 1413–1434. https://doi.org/10.1007/s11033-019-05230-7.
(9) Wang, X.-W.; Liu, C.-X.; Chen, L.-L.; Zhang, Q. C. RNA Structure Probing Uncovers RNA Structure-Dependent Biological Functions. *Nature Chemical Biology* **2021**, *17* (7), 755–766. https://doi.org/10.1038/s41589-021-00805-7.
(10) Zhong, Y.; Hyung, S.-J.; Ruotolo, B. T. Ion Mobility–Mass Spectrometry for Structural Proteomics. *Expert Review of Proteomics* **2012**, *9* (1), 47–58. https://doi.org/10.1586/epr.11.75.
(11) Fabris, D. CHAPTER 17. Ion Mobility–Mass Spectrometry of Nucleic Acids. *Ion Mobility-Mass Spectrometry* **2021**, 461–495. https://doi.org/10.1039/9781839162886-00461.
(12) Kenderdine, T.; Fabris, D. The Multifaceted Roles of Mass Spectrometric Analysis in Nucleic Acids Drug Discovery and Development. *Mass Spectrometry Reviews* **2021**. https://doi.org/10.1002/mas.21766.
(13) Largy, E.; König, A.; Ghosh, A.; Ghosh, D.; Benabou, S.; Rosu, F.; Gabelica, V. Mass Spectrometry of Nucleic Acid Noncovalent Complexes. *Chemical Reviews* **2021**, *122* (8), 7720–7839. https://doi.org/10.1021/acs.chemrev.1c00386.
(14) Ruotolo, B. T.; Benesch, J. L. P.; Sandercock, A. M.; Hyung, S.-J.; Robinson, C. V. Ion Mobility–Mass Spectrometry Analysis of Large Protein Complexes. *Nature Protocols* **2008**, *3* (7), 1139–1152. https://doi.org/10.1038/nprot.2008.78.
(15) Dixit, S. M.; Polasky, D. A.; Ruotolo, B. T. Collision Induced Unfolding of Isolated Proteins in the Gas Phase: Past, Present, and Future. *Current Opinion in Chemical Biology* **2018**, *42*, 93–100. https://doi.org/10.1016/j.cbpa.2017.11.010.
(16) Eschweiler, J. D.; Martini, R. M.; Ruotolo, B. T. Chemical Probes and Engineered Constructs Reveal a Detailed Unfolding Mechanism for a Solvent-Free Multidomain Protein. *Journal of the American Chemical Society* **2016**, *139* (1), 534–540. https://doi.org/10.1021/jacs.6b11678.
(17) Zhong, Y.; Han, L.; Ruotolo, B. T. Collisional and Coulombic Unfolding of Gas-Phase Proteins: High Correlation to Their Domain Structures in Solution. *Angewandte Chemie* **2014**, *126* (35), 9363–9366. https://doi.org/10.1002/ange.201403784.
(18) Tian, Y.; Han, L.; Buckner, A. C.; Ruotolo, B. T. Collision Induced Unfolding of Intact Antibodies: Rapid Characterization of Disulfide Bonding Patterns, Glycosylation, and Structures. *Analytical Chemistry* **2015**, *87* (22), 11509–11515. https://doi.org/10.1021/acs.analchem.5b03291.
(19) Rabuck-Gibbons, J. N.; Keating, J. E.; Ruotolo, B. T. Collision Induced Unfolding and Dissociation Differentiates ATP-Competitive from Allosteric Protein Tyrosine Kinase Inhibitors. *International Journal of Mass Spectrometry* **2018**, *427*, 151–156. https://doi.org/10.1016/j.ijms.2017.12.002.
(20) Politis, A.; Park, A. Y.; Hall, Z.; Ruotolo, B. T.; Robinson, C. V. Integrative Modelling Coupled with Ion Mobility Mass Spectrometry Reveals Structural Features of the Clamp Loader in Complex with Single-Stranded DNA Binding Protein. *Journal of Molecular Biology* **2013**, *425* (23), 4790–4801. https://doi.org/10.1016/j.jmb.2013.04.006.
(21) Serganov, A.; Huang, L.; Patel, D. J. Coenzyme Recognition and Gene Regulation by a Flavin Mononucleotide Riboswitch. *Nature* **2009**, *458* (7235), 233–237. https://doi.org/10.1038/nature07642.
(22) Milligan, J. F.; Groebe, D. R.; Witherell, G. W.; Uhlenbeck, O. C. Nucleic Acids Research Oligoribonucleotide Synthesis Using T7 RNA Polymerase and Synthetic DNA Templates. *Nucleic Acids Res* **1987**, *15* (21).
(23) Hendry, P.; Hannan, G. Detection and Quantitation of Unlabeled Nucleic in Polyacrylamide Gels. *Biotechniques* **1996**, *20* (2), 258–264.
(24) Hossain, M.; Suresh Kumar, G. DNA Intercalation of Methylene Blue and Quinacrine: New Insights into Base and Sequence Specificity from Structural and Thermodynamic Studies with Polynucleotides. *Mol Biosyst* **2009**, *5* (11), 1311–1322. https://doi.org/10.1039/b909563b.
(25) Konermann, L.; Ahadi, E.; Rodriguez, A. D.; Vahidi, S. Unraveling the Mechanism of Electrospray Ionization. *Analytical Chemistry* **2012**, *85* (1), 2–9. https://doi.org/10.1021/ac302789c.
(26) Marty, M. T.; Baldwin, A. J.; Marklund, E. G.; Hochberg, G. K. A.; Benesch, J. L. P.; Robinso–n, C. V. Bayesian Deconvolution of Mass and Ion Mobility Spectra: From Binary Interactions to Polydisperse Ensembles. *Analytical Chemistry* **2015**, *87* (8), 4370–4376. https://doi.org/10.1021/acs.analchem.5b00140.
(27) Gadkari, V. V.; Ramírez, C. R.; Vallejo, D. D.; Kurulugama, R. T.; Fjeldsted, J. C.; Ruotolo, B. T. Enhanced Collision Induced Unfolding and Electron Capture Dissociation of Native-like Protein Ions. *Analytical Chemistry* **2020**, *92* (23), 15489–15496. https://doi.org/10.1021/acs.analchem.0c03372.
(28) Gadkari, V. V.; Juliano, B. R.; Mallis, C. S.; May, J. C.; Kurulugama, R. T.; Fjeldsted, J. C.; McLean, J. A.; Russell, D. H.; Ruotolo, B. T. Performance Evaluation of In-Source Ion Activation Hardware for Collision-Induced Unfolding of Proteins and Protein Complexes on a Drift Tube Ion Mobility-Mass Spectrometer. *The Analyst* **2023**, *148* (2), 391–401. https://doi.org/10.1039/d2an01452a.
(29) Polasky, D. A.; Dixit, S. M.; Fantin, S. M.; Ruotolo, B. T. CIUSuite 2: Next-Generation Software for the Analysis of Gas-Phase Protein

Unfolding Data. *Analytical Chemistry* **2019**, *91* (4), 3147–3155. https://doi.org/10.1021/acs.analchem.8b05762.
(30) Hall, Z., Politis, A., Bush, M. F., Smith, L. J., & Robinson, C. V. (2012). Charge-state dependent compaction and dissociation of protein complexes: Insights from Ion Mobility and molecular dynamics. *Journal of the American Chemical Society*, *134*(7), 3429–3438. https://doi.org/10.1021/ja2096859.
(31) Heilman-Miller, S. L.; Thirumalai, D.; Woodson, S. A. Role of Counterion Condensation in Folding of the Tetrahymena Ribozyme. I. Equilibrium Stabilization by Cations. *Journal of Molecular Biology* **2001**, *306* (5), 1157–1166. https://doi.org/10.1006/jmbi.2001.4437.
(32) Lipfert, J.; Doniach, S.; Das, R.; Herschlag, D. Understanding Nucleic Acid–Ion Interactions. *Annual Review of Biochemistry* **2014**, *83* (1), 813–841. https://doi.org/10.1146/annurev-biochem-060409-092720.
(33) Ileka, K. Structural Characterization of Ribonucleic Acids and Their Complexes by Negative-ion Mode Mass Spectrometry (Ph.D. and Master's Collections), 2018. Available from DeepBlue Dissertations and Theses Database.
(34) Abi-Ghanem, J.; Rabin, C.; Porrini, M.; Rosu, F.; Gabelica, V. Compaction of RNA Hairpins and Their Kissing Complexes in Native Electrospray Mass Spectrometry. ASMS **2020**. https://doi.org/10.26434/chemrxiv.11876505.
(35) Porrini, M.; Rosu, F.; Rabin, C.; Darré, L.; Gómez, H.; Orozco, M.; Gabelica, V. Compaction of Duplex Nucleic Acids upon Native Electrospray Mass Spectrometry. *ACS Central Science* **2017**, *3* (5), 454–461. https://doi.org/10.1021/acscentsci.7b00084.
(36) Reznichenko, O.; Cucchiarini, A.; Gabelica, V.; Granzhan, A. Quadruplex DNA-Guided Ligand Selection from Dynamic Combinatorial Libraries of Acylhydrazones. *Organic & Biomolecular Chemistry* **2021**, *19* (2), 379–386. https://doi.org/10.1039/d0ob01908a.
(37) Paul, D.; Marchand, A.; Verga, D.; Teulade-Fichou, M.-P.; Bombard, S.; Rosu, F.; Gabelica, V. Probing Ligand and Cation Binding Sites in G-Quadruplex Nucleic Acids by Mass Spectrometry and Electron Photodetachment Dissociation Sequencing. *The Analyst* **2019**, *144* (11), 3518–3524. https://doi.org/10.1039/c9an00398c.
(38) Turner, K. B.; Brinson, R. G.; Yi-Brunozzi, H. Y.; Rausch, J. W.; Miller, J. T.; Le Grice, S. F. J.; Marino, J. P.; Fabris, D. Structural Probing of the HIV-1 Polypurine Tract RNA:DNA Hybrid Using Classic Nucleic Acid Ligands. *Nucleic Acids Research* **2008**, *36* (8), 2799–2810. https://doi.org/10.1093/nar/gkn129.
(39) Yamagami, R.; Sieg, J. P.; Bevilacqua, P. C. Functional Roles of Chelated Magnesium Ions in RNA Folding and Function. *Biochemistry* **2021**, *60* (31), 2374–2386. https://doi.org/10.1021/acs.biochem.1c00012.
(40) Liu, X.; Wu, N.; Shanmuganathan, A.; Klemm, B. P.; Howard, M. J.; Lim, W. H.; Koutmos, M.; Fierke, C. A. Kinetic Mechanism of Human Mitochondrial RNase P. **2019**. https://doi.org/10.1101/666792.
(41) Karasik, A.; Fierke, C. A.; Koutmos, M. Disease Associated Mutations in Mitochondrial Precursor TRNAs Affect Binding, M1R9 Methylation and TRNA Processing by MtRNase P. **2020**. https://doi.org/10.1101/2020.07.07.191726.
(42) Strulson, C. A.; Boyer, J. A.; Whitman, E. E.; Bevilacqua, P. C. Molecular Crowders and Cosolutes Promote Folding Cooperativity of RNA under Physiological Ionic Conditions. *RNA* **2014**, *20* (3), 331–347. https://doi.org/10.1261/rna.042747.113.
(43) Wilt, H. M., Yu, P., Tan, K., Wang, Y.-X., & Stagno, J. R. (2020). FMN riboswitch aptamer symmetry facilitates conformational switching through mutually exclusive coaxial stacking configurations. *Journal of Structural Biology: X*, *4*, 100035. https://doi.org/10.1016/j.yjsbx.2020.100035
(44)Grilley, D.; Soto, A. M.; Draper, D. E. Chapter 3 Direct Quantitation of Mg2+-RNA Interactions by Use of a Fluorescent Dye. *Methods in Enzymology* **2009**, 71–94. https://doi.org/10.1016/s0076-6879(08)04203-1.
(45)Grilley, D.; Soto, A. M.; Draper, D. E. Chapter 3 Direct Quantitation of Mg2+-RNA Interactions by Use of a Fluorescent Dye. *Methods in Enzymology* **2009**, 71–94.
(42-46) Misra VK, Draper DE. On the role of magnesium ions in RNA stability. Biopolymers. 1998;48(2-3):113-35. doi: 10.1002/(SICI)1097-0282(1998)48:2<113::AID-BIP3>3.0.CO;2-Y. PMID: 10333741.https://doi.org/10.1016/s0076-6879(08)04203-1.
(47) SERRA, M. J.; BAIRD, J. D.; DALE, T.; FEY, B. L.; RETATAGOS, K.; WESTHOF, E. Effects of Magnesium Ions on the Stabilization of RNA Oligomers of Defined Structures. *RNA* **2002**, *8* (3), 307–323. https://doi.org/10.1017/s1355838202024226.
(48)Nobles, K. N. Highly Conserved Modified Nucleosides Influence Mg2+-Dependent TRNA Folding. *Nucleic Acids Research* **2002**, *30* (21), 4751–4760. https://doi.org/10.1093/nar/gkf595.
(49) Saha, A.; Nandi, N. Role of the Transfer Ribonucleic Acid (TRNA) Bound Magnesium Ions in the Charging Step of Aminoacylation Reaction in the Glutamyl TRNA Synthetase and the Seryl TRNA Synthetase Bound with Cognate TRNA. *Journal of Biomolecular Structure and Dynamics* **2021**, 1–22. https://doi.org/10.1080/07391102.2021.1914732.
(50) HOLLEY, R. W.; APGAR, J.; EVERETT, G. A.; MADISON, J. T.; MARQUISEE, M.; MERRILL, S. H.; PENSWICK, J. R.; ZAMIR, A. STRUCTURE of a RIBONUCLEIC ACID. *Science (New York, N.Y.)* **1965**, *147* (3664), 1462–1465. https://doi.org/10.1126/science.147.3664.1462.
(51) Schauss, J.; Kundu, A.; Fingerhut, B. P.; Elsaesser, T. Magnesium Contact Ions Stabilize the Tertiary Structure of Transfer RNA: Electrostatics Mapped by Two-Dimensional Infrared Spectra and Theoretical Simulations. *The Journal of Physical Chemistry B* **2020**, *125* (3), 740–747. https://doi.org/10.1021/acs.jpcb.0c08966.
(52) Suzuki, T.; Nagao, A.; Suzuki, T. Human Mitochondrial TRNAs: Biogenesis, Function, Structural Aspects, and Diseases. *Annual Review of Genetics* **2011**, *45* (1), 299–329. https://doi.org/10.1146/annurev-genet-110410-132531.
(53) Yarham, J. W.; Elson, J. L.; Blakely, E. L.; McFarland, R.; Taylor, R. W. Mitochondrial TRNA Mutations and Disease. *Wiley interdisciplinary reviews. RNA* **2010**, *1* (2), 304–324. https://doi.org/10.1002/wrna.27.
(54) Tuppen, H. A. L.; Blakely, E. L.; Turnbull, D. M.; Taylor, R. W. Mitochondrial DNA Mutations and Human Disease. *Biochimica et Biophysica Acta (BBA) - Bioenergetics* **2010**, *1797* (2), 113–128. https://doi.org/10.1016/j.bbabio.2009.09.005.
(55) Thornlow, B. P.; Hough, J.; Roger, J. M.; Gong, H.; Lowe, T. M.; Corbett-Detig, R. B. Transfer RNA Genes Experience Exceptionally Elevated Mutation Rates. **2017**. https://doi.org/10.1101/229906.
(56) Sheng, B.; Fong, M. K.; Kwan Ng, W.; Lam Chen, S. P.; Miu Mak, C. MELAS, MIDD and Beyond: M.3243A>G MT-TL1 Mutation in Adult Patients. *International Journal of Clinical Medicine* **2016**, *07* (07), 487–495. https://doi.org/10.4236/ijcm.2016.77054.
(57) Lin, D.-S.; Huang, Y.-W.; Ho, C.-S.; Huang, T.-S.; Lee, T.-H.; Wu, T.-Y.; Huang, Z.-D.; Wang, T.-J. Impact of Mitochondrial A3243G Heteroplasmy on Mitochondrial Bioenergetics and Dynamics of Directly Reprogrammed MELAS Neurons. *Cells* **2022**, *12* (1), 15. https://doi.org/10.3390/cells12010015.
(58) D'Souza, Aaron R.; Minczuk, M. Mitochondrial Transcription and Translation: Overview. *Essays in Biochemistry* **2018**, *62* (3), 309–320. https://doi.org/10.1042/ebc20170102.
(59) Liu, X.; Wu, N.; Shanmuganathan, A.; Klemm, B. P.; Howard, M. J.; Lim, W. H.; Koutmos, M.; Fierke, C. A. Kinetic Mechanism of Human Mitochondrial RNase P. **2019**. https://doi.org/10.1101/666792.
(56-60) Wittenhagen, L. M.; Kelley, S. O. Dimerization of a Pathogenic Human Mitochondrial TRNA. *Nature Structural Biology* **2002**. https://doi.org/10.1038/nsb820.

(61) Machnicka, M. A.; Olchowik, A.; Grosjean, H.; Bujnicki, J. M. Distribution and Frequencies of Post-Transcriptional Modifications in TRNAs. *RNA Biology* **2014**, *11* (12), 1619–1629. https://doi.org/10.4161/15476286.2014.992273.
(62) Suzuki, T.; Suzuki, T. A Complete Landscape of Post-Transcriptional Modifications in Mammalian Mitochondrial TRNAs. *Nucleic Acids Research* **2014**, *42* (11), 7346–7357. https://doi.org/10.1093/nar/gku390.